Automatic Analysis of Aqueous Specimens for Phytoplankton Structure Recognition and Population Estimation

KARSTEN RODENACKER,[1*] BURKHARD HENSE,[1] UTA JÜTTING,[1] AND PETER GAIS[2]
[1]*Institute of Biomathematics and Biometry, GSF-National Research Center for Environment and Health, Neuherberg 85764, Germany*
[2]*Institute of Pathology, GSF-National Research Center for Environment and Health, Neuherberg 85764, Germany*

KEY WORDS Utermöhl plankton chambers; digital image analysis; fluorescence analysis; quantification; image archiving system

ABSTRACT An automatic microscope image acquisition, evaluation, and recognition system was developed for the analysis of Utermöhl plankton chambers in terms of taxonomic algae recognition. The system called PLASA (Plankton Structure Analysis) comprises (1) fully automatic archiving (optical fixation) of aqueous specimens as digital bright field and fluorescence images, (2) phytoplankton analysis and recognition, and (3) training facilities for new taxa. It enables characterization of aqueous specimens by their populations. The system is described in detail with emphasis on image analytical aspects. Plankton chambers are scanned by sizable grids, divers objective(s), and up to four fluorescence spectral bands. Acquisition positions are focused and digitized by a TV camera and archived on disk. The image data sets are evaluated by a large set of quantitative features. Automatic classifications for a number of organisms are developed and embedded in the program. Interactive programs for the design of training sets were additionally implemented. A long-term sampling period of 23 weeks from two ponds at two different locations each was performed to generate a reliable data set for training and testing purposes. These data were used to present this system's results for phytoplankton structure characterization. PLASA represents an automatic system, comprising all steps from specimen processing to algae identification up to species level and quantification. *Microsc. Res. Tech. 69:708–720, 2006.*

INTRODUCTION

Investigations of population dynamics in phytoplankton communities are an important part of many ecological and ecotoxicological problems. Because of phytoplankton complexity, taxonomic identification and quantification tend to be work and time intensive and therefore costly, making integration of automated steps desirable (Gaston and O'Neill, 2004). The initial reason for the development presented here was an ecotoxicological microcosm study, lasting over several years and requiring the analysis of a huge amount of similar phytoplankton samples each year (Hense et al., 2003, 2004).

Analytical methods with integrative density measurements such as photometric, up to flow cytometry, improve the investigation of phytoplankton communities. However, these methods are restricted in taxonomical discrimination (Franqueira et al., 2000; Steinberg et al., 1996). Digital image analysis has a greater potential for discrimination, but shortcomings have limited our attempts of integrating this method into phytoplankton research until now (Bayerand et al., 2001; Gray et al., 2002; Rines, 1999; Walker, 1999; Walker et al., 1998, 2002). Samples taken from natural ecosystems often contain high numbers of objects in addition to living phytoplankton cells, i.e., zooplankton, detritus, and inorganic particles. Also, the multitude of various forms and sizes make unambiguous identification of phytoplankton difficult. As described in Gaston and O'Neill (2004), a high number of phytoplankton species impede identification by reason of nondifferentiability or of a missing taxonomic order.

An appropriate integration of fluorescence imaging into digital image analysis procedures should improve the situation. Fluorescence has two capabilities for phytoplankton: First, because of its content of chlorophyll, phytoplankton emits specific autofluorescence. This allows a separation of living phytoplankton cells from nearly all other structures. Second, in different algae classes, different accessory pigments occur with different fluorescence characteristics (Larkum et al., 2003; Rowan, 1989). In principle, three phytoplankton groups with a different complement of pigments with different spectral properties can be described (Babichenko et al., 1999; Steinberg et al., 1996): (1) groups containing phycoerythrin (PE) (in freshwater species of Cyanophyceae and Cryptophyceae), (2) groups with predominantly chlorophyll (in freshwater Chlorophyceae, Euglenophyceae, and Conjugatophyceae), and (3) groups with high carotinoid content (in freshwater Chrysophyceae, Bacillariophyceae, and Dinophyceae). Carotinoids were excited at specific wave lengths, but emit fluorescence via fluorescence energy transfer to the chlorophyll or longer wavelength pigments.

Previous tests showed that discrimination of fluorescence with excitation by mercury light is possible for

*Correspondence to: K. Rodenacker, Institute of Biomathematics and Biometry, GSF-National Research Center for Environment and Health, Neuherberg 85764, Germany. E-mail: karsten.rodenacker@gsf.de

Received 17 September 2005; accepted 1 April 2006
Contract grant sponsor: GSF.
DOI 10.1002/jemt.20338
Published online 4 August 2006 in Wiley InterScience (www.interscience.wiley.com).

chlorophyll- and PE-containing cells. Various chlorophylls exist in algae with slightly different fluorescence spectra. Chlorophyll a is present in (almost) all plants, whereas the chlorophylls b, c, and d occur in different specific amounts per cell in some algae classes (for details see Larkum et al., 2003; Rowan, 1989). The approach in PLASA (Plankton Structure Analysis) integrates fluorescence information of all chlorophylls. However, as chlorophyll a is generally the predominant form, present in almost all algae, and the energy absorbed by the other chlorophylls is mostly transferred to chlorophyll a (Formaggio et al., 2001), we use the term chlorophyll a in the following descriptions. Chlorophyll a autofluorescence emits maximum light at wave lengths around 680 nm with excitation around 430–490 nm. PE is excited at higher wave length above 500 nm and emits fluorescence primarily around 580–590 nm.

In this paper, we present an automatic archiving and analysis system (PLASA) composed of a fully automated image acquisition system using standard specimen holders (optical fixation from Utermöhl plankton chambers) and an also fully automated digital image analysis. The image analysis methods are described in Appendix. Additionally, some results from long-running sampling time periods have quantitated algae total density and total fluorescence as well as the first results from our classifiers for selected species. The goal of the classifiers was to gather a representative set of image data reflecting the phytoplankton community structure over the main growth phase of one year to test the long-term stability of the gathering device over a long-term sampling period, to document the value of fluorescence data improved phytoplankton community identification and quantification, and to have a considerable large pool of algae individuals to test our classifications.

MATERIALS AND METHODS

Pelagic samples from aquatic ecosystems were taken weekly in the year 2003 from week 25 to week 45 as well as from two ponds at two locations each about 4 m apart with samples gathered at a depth of 10 cm. Pond 1 is located inside the campus of the GSF Research Center, 9 m × 6 m, 1.20 m deep, open and densely covered with water plants, the other a small garden pond, Pond 2 is about 10 m × 3 m, max. 1 m deep, shadowed by bushes with very few water plants. Samples were fixed with 0.1% glutaraldehyde (Merck, Darmstadt, Germany, http://www.merck.de) to preserve autofluorescence and gravity sedimented in plankton chambers for 24 h. Similar to manual analysis, the sample volume was chosen so that the sedimented cells lie on the bottom of the plankton chamber and do not occlude each other. This was done by estimating the density in the unfixed, living samples in a microscope. Usually, between 20 and 50 mL water was sedimented. Some samples contain amounts of large, nonphytoplankton particles, especially in autumn, when degradation activity leads to increasing numbers of detritus. To improve processing in image analysis, such samples were filtered using 63 μm grid hole sizes. The samples were then automatically scanned following the Utermöhl method (Lund et al., 1958; Utermöhl, 1958) using an inverse microscope (see Fig. 1). For the design of a classification system, the following organisms were selected: *Peridinium umbonatum* (PEUM), *Cryptomonas erosa* (CRER), *Cryptomonas marsonii* (CRMA), *Trachelomonas* sp. (ROTT), and *Ankistrodesmus* sp. (WURM).

Image Acquisition Method (Optical Fixation)

Image acquisition is performed with a computerized inverse microscope DM IRBE (Leica, Bensheim, Germany, http://www.leica-microsystems.com) and a 3-chip CCD color TV camera KY-F58 (JVC, Tokyo, Japan, http://www.jvc.com). To be able to evaluate algae species of various sizes, magnifications using the objectives 10× N-Plan, n.a. 0.22, 20× N-Plan, n.a. 0.4, 40× N-Plan, n.a. 0.55, and 63× Plan-Fluotar, n.a. 0.70 were chosen.

For fluorescence image acquisition, two filter sets were used: (a) I_3: Excitation filter BP 450–490, dichroic reflector 510, emission filter LP 515 and (b) N_3: Excitation filter BP 546/12, dichroic reflector 565, emission filter BP 600/40. Filter set N_3 shows PE fluorescence, but not chlorophyll a. Filter set I_3 has a broad emission range. It includes chlorophyll a, but also fluorescence from shorter wavelengths. This may not seem to be desirable, but additional emission wavelengths provide additional information. For example, chlorophyll a, which is the dominant pigment in algae, tends to emit more yellow light than red when stored for a long time.

The acquisition process from changing the objective, auto-focus, lamp voltage control, and stage movements for image gathering up to image storage are controlled by a lab-developed procedure using the microscope firmware QWIN Version 2.6 (Leica, Bensheim, Germany, http://www.leica-microsystems.com). The digitized images were stored as image files in TIFF file format on computer disk each with a size of 760 × 576 pixel. The pixel size amounts for the two main magnifications, to 0.316 μm for the 40× and to 0.632 μm for the 20× objective, respectively.

Setup. Before starting the automatic acquisition process, magnifications were chosen (10×, 20×, 40×, 63×), scanning path (meander, spiral (Fig. 1), random) was selected, and density (number of scan points) was set. Then, camera or digitization parameters (brightness, offset, and gain) were adjusted respectively for the actual specimen. Additionally, for each magnification, a white background image (bright field, BF) is acquired for shading and color correction purposes. Correction by means of these background images can mostly eliminate shading, color gradients, failures in color correction, color of the sampling water, and spots caused by pollution in the optical system.

To obtain well-focused images due to uneven glass slides, a multistage process is applied. First, a focus map is generated by the interpolation of a number of interactively adjusted points distributed evenly over the scanning field using a thin-plate spline, considered as two-dimensional extension of cubic splines. The resulting height map is then used for each scan point as the starting focus setting (Fig. 2). Spiral path was mostly chosen for scanning. An autofocus range of 20 μm (in some cases 40 μm) and an autofocus step size of 2 μm were used. A threshold was used to reject all

Fig. 1. Uthermöhl chamber with overlayed scanned images and scanning path.

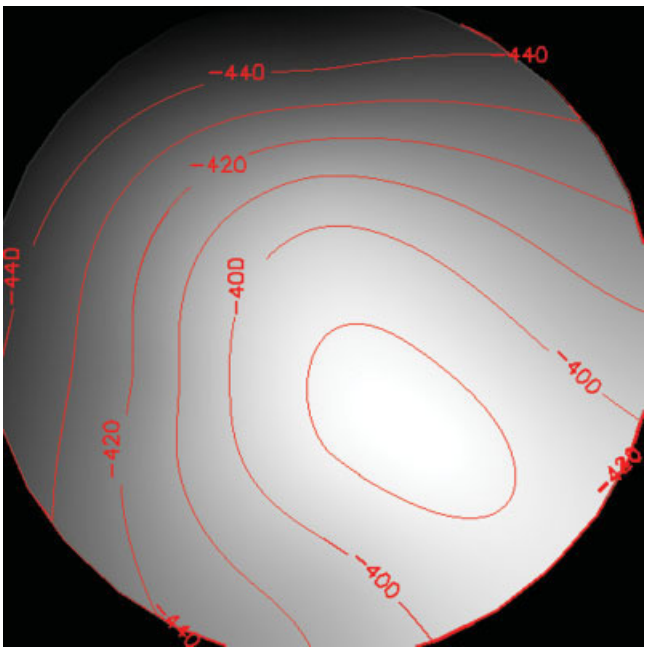

Fig. 2. Focus map of a plankton chamber for initial focus estimate. Focal depth contour lines marked in micrometers.

images with mean gray values below 128, as too dark for image analysis.

Acquisition Process. For each chosen magnification, the specimen is scanned. At each position, BF images are stored as RGB-images in TIFF format. Fluorescence intensities are spectrally separated by the

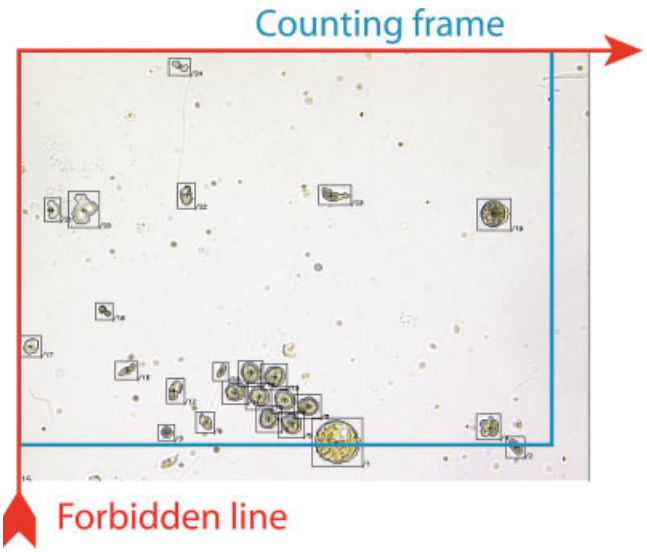

Fig. 3. Illustration of the counting and measurement rule inside the counting frame.

TV-camera into $R_{I3}G_{I3}B_{I3}$ and $R_{N3}G_{N3}B_{N3}$ from the two filter sets I_3 and N_3. Channels $R_{I3}G_{I3}R_{N3}$ are stored in a second RGB-TIFF-image. In other words, a new composite fluorescence image with red and green channel from filter I_3 (chlorophyll a) and blue channel from red channel of filter N_3 (PE) is stored.

During processing of autofocus, we experienced a random shift of focal z-axis position, a loss of the actual position. To catch again in-focus position after a fixed number of scanned images, a previously defined point is relocated and automatically refocused. Refocussing during acquisition was conducted every 15 acquired scanning points. The difference between the previous focus position at this point and the actual one found is used for correction of the estimated focus position from the focus map mentioned above. After setting this second estimate, the microscope's built-in autofocus procedure is applied.

Data Processing Method

The whole program is implemented in IDL (Interactive Data Language, Research Systems, Boulder, CO 80301, http://www.rsinc.com). The program comprises a graphical user interface with extended display and interaction capabilities that allow the definition of algae training sets with the ability to interactively control and improve segmentation. Additionally, several possibilities exist to define algae type classes, classification schemes, and display of algae galleries. Feature calculation methods of objects are partially described in Rodenacker and Bengtsson (2003) and outlined in Appendix.

Preprocessing, Shading, and Color Correction. Digitized color images from transmitted light are dependent on a multitude of factors besides the actual material in the light path. The most important factors are the light source (color temperature, spectral dependent refraction), the optical system, especially mal-

adjustments and particles in the light paths, and the sensor of the TV camera. It is not possible to correct all these influences. However, using the previously acquired background image RGB_{WB}, the shading and color correction functions are calculated and applied to each BF image. To preserve the visual impression of the BF images, color processing according to ITU-R BT.709 (1990) was followed. Global BF intensity (gray) I is calculated by the formula $I = 0.2126 \times R + 0.7152 \times G + 0.0722 \times B$ instead of using equally weighted color channels. Shading correction is done with I_{WB}. Color corrections are performed using the respective color channels R_{WB}, G_{WB}, and B_{WB}.

Segmentation. Segmentation was achieved by a two step procedure. (1) The background of the corrected image I is so homogeneous that a good rough segmentation could be achieved sufficiently by one intensity threshold. For noisy specimens, an image filtering on the base of mathematical morphology or linear analysis (low pass filtering) can be applied before the threshold is calculated. With our data, the latter was used. Actually, the most frequent pixel value of the intensity image I, the $md(I)$, is assumed as the BF background. This value is reduced by a multiple of the estimated background standard deviation that serves as first threshold. The resulting mask is morphologically closed by a 4-connected  structuring element, hole filled, and then opened by inclined 4-connected  structuring elements (Serra, 1982). This joins small gaps in the object contour and deletes isolated point configurations. (2) For fine segmentation, the selected object is cut out with a slightly enlarged window and again segmented by a threshold. This threshold models the histogram of intensity pixel values from the object box by a Gaussian and a second-order polynomial. If this method fails, the robust automatic threshold RAT (Kittler et al., 1985) is applied. The resulting mask image is again slightly cleaned as described in the previous section. No dissection of overlapping or occluding organisms is performed.

To allow an unbiased estimate of organism frequencies and volume fractions, the so-called forbidden line algorithm is applied (see Fig. 3). All objects touching this line are not accepted for further evaluation. The counting and measurement frame is defined by a reduced image frame, the don't care zone, where the lower and right border are defined at a certain distance. Objects only inside the don't care zone are rejected.

Featuring. After segmentation and object rejection for unbiased counting, each found object is represented by the set of pixels occupying the respective image area (area-based representation) and by its contour as the ordered list of contour pixel coordinates (contour-based representation). For the different feature extraction methods, the most adequate object representation is used. About 200 numeric features are actually calculated, see Appendix for description and illustration. There seems to be a large number of features; however, the differences of organisms are multiple and the organisms to be detected should not be limited by the features chosen.

The features are grouped into morphometric, densitometric, colorimetric, and fluorometric features. Emphasis is laid on the first group of features. Morphological or shape criteria are much more difficult to apply compared with the other feature groups in terms of quantification and also in terms of visual discrimination. We calculate from the masks of the detected objects features summarized as general shape (especially size parameters), significant points (location and distances between such points), principal component analysis (PCA), Fourier based descriptors from the complex contour frequency spectrum (FFT) (da Fontoura Costa and Cesar, 2001), (invariant) shape moments (Hu, 1962; Reiss, 1993), and Freeman contour code. The calculated features are listed and partially illustrated in Appendix. Besides the mere quantitative description of shape properties, we are faced with the problems of object segmentation. Often, organelles or slimy artifacts near organism borders lead to disturbed segmentations. Hence, we have to group the morphological features that are more or less sensitive to segmentation artifacts. Such feature properties are, of course, not in every case advantageous.

For densitometry measurements, the intensity image I (ITU-R BT.709, 1990) is calculated into extinction values E (see Appendix Table A2), directly related to the amount of material in the light path. For colorimetry, the RGB image is transformed into the well-known HLS-System (hue, luminance, saturation) and additionally into the Lch-System (luminance, chromaticity, hue) following again the recommendations CIE_Lab or CIE_Lch (ITU-R BT.709, 1990), respectively. Lch-System and especially hue (h) are similar to human color discrimination.

Fluorescence images often show shades resulting from TV camera effects. To reduce such shades from the original fluorescence intensity image a low pass filtered version of the fluorescence image is subtracted for special fluorescence shading correction. The low pass filter size is fixed to the size of the don't care zone of the forbidden line algorithm (see above), e.g., 16 μm or about 50 pixel in the 40× objective. For intensity measurements, the corrected fluorescence intensity is logarithmically transformed similar to the calculation of extinction (see Appendix Table A4).

From extinction E, hue H, luminance L, saturation S (from HLS-system), luminance L_1, chromaticity C, hue H_1 (from Lch-system), and from the possible four fluorescence channels $F_{1.4,}$ respective pixel values the mean ($M1$), variance ($M2$), skewness ($M3$), and excess ($M4$) were calculated. Some illustrations for this set of features are given in Appendix Tables A2 and A3. All features are based on the area representation, since pixel properties are used.

Training and Design of Classifier. Training sets for various organisms are generated by interactive selection from the 40× objective samples. An extensive graphical user interface is implemented, allowing various tasks (see Fig. 4) using visual and numerical inspection. The necessary and/or feasible size of the training sets depends on the heterogeneity of the respective organisms. It has to be adjusted in terms of selectivity and specificity and cannot be generalized. Even the creation of artificial nontaxonomical related subgroups was used to obtain improved

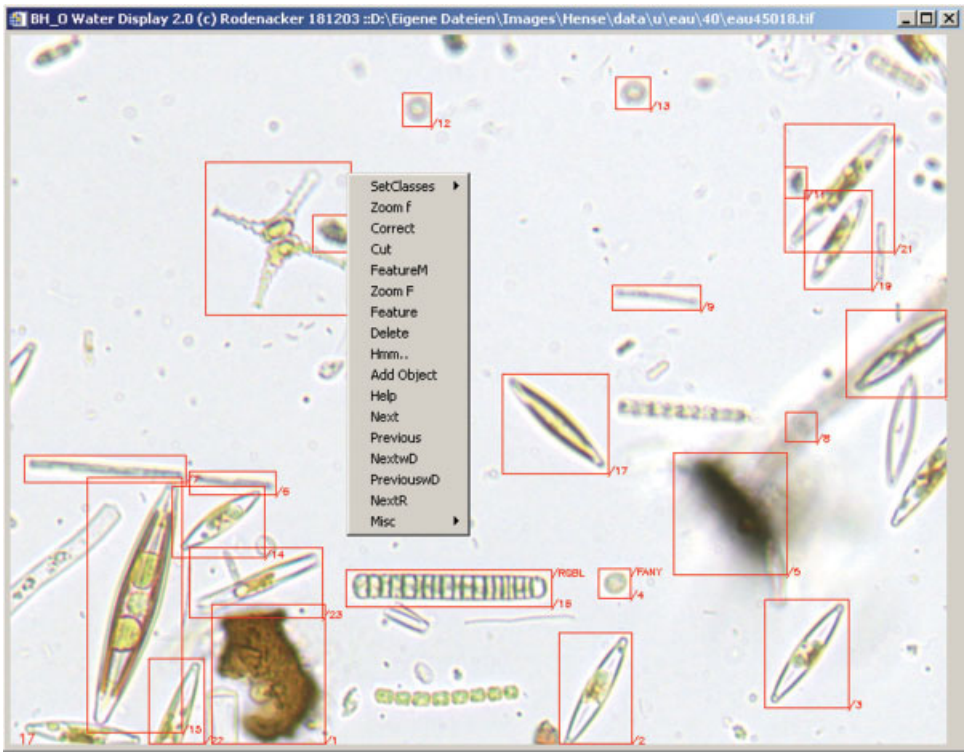

Fig. 4. Image display window with marked objects and context pull-down menu.

results in subsequent classification steps. Based on these training sets of organisms, a classifier is constructed. For an exemplary analysis, five organisms are selected from the whole data set by rough classifications using already known features like area, fluorescence, and optical density. The result is visually controlled and corrected. Additional new transformation features are added and all size features are normalized from pixel to micrometer using the application of the classifiers for other magnifications too. The complete feature data set with the defined classes is analyzed using SAS (The SAS System, SAS Institute, Cary, NC, http://www.sas.com).

The following steps build a hierarchical classifier: (1) Maxima and minima for the known important features are set for each algae class. (2) A 2-class stepwise linear discriminant analysis (LDA) is performed for each class versus all remaining algae. (3) For the chosen features, the set limits are already readjusted, (4) followed by another stepwise LDA. (5) For each class, the results are visually inspected using the display system (see Figs. 5 and 6). This procedure is iterated until the results are satisfactory. The resulting classifier represents a tree classifier with a combination of uni- and multivariate classification steps.

RESULTS

Processing Time

The acquisition procedure needs about 7–15 min time for interactive initiation. Each acquired scanning position takes 70–90 s on average, of which about 7 s are needed for the actual image acquisition. Most of the time (>90%) is required by the autofocus routine. Smaller autofocus ranges could improve it, but with the drawback of a higher proportion of focus failures. An improvement of autofocus software to hasten it is at the moment limited by the random z-shift of our microscope. The evaluation time for object segmentation and

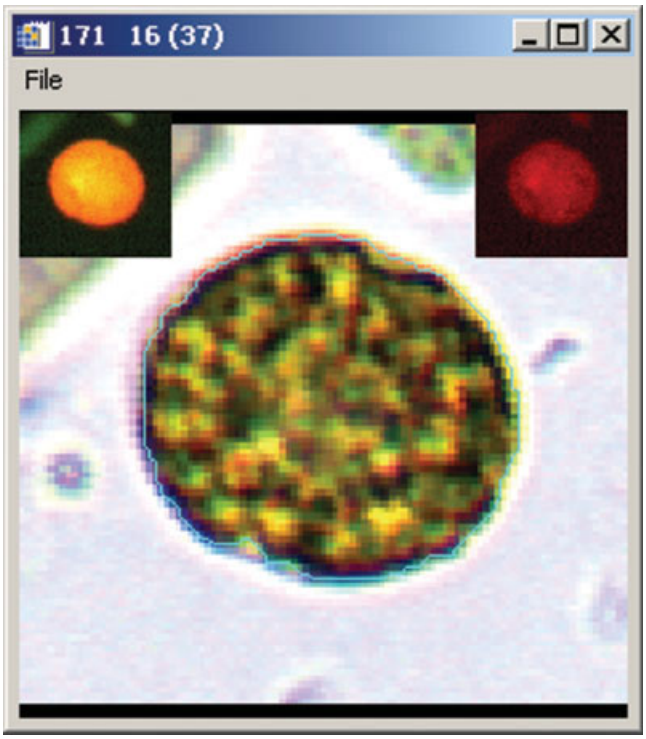

Fig. 5. *P. umbonatum* with fluorescent thumbnails (upper left chlorophyll a, upper right PE fluorescence) and segmentation contour.

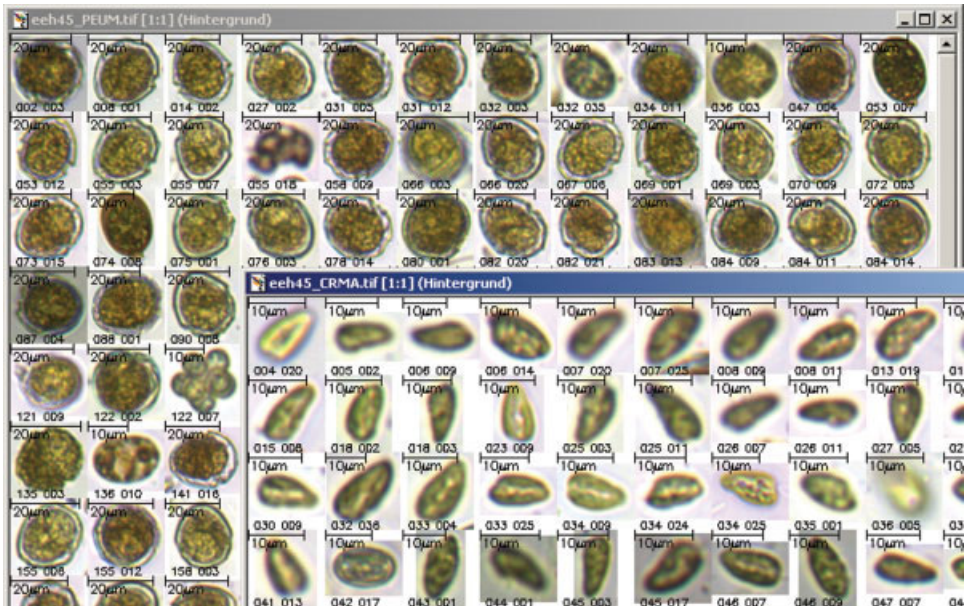

Fig. 6. Gallery example of mostly *P. umbonatum* and *C. marsonii*. Each alga is scaled and accompanied by an individual scale.

feature calculation depends on the numerical density of objects inside the image frame, with a PC, 3 GHz, 5–45 s per scanning position is required.

Automatic Image Acquisition

Quality of image acquisition was analyzed in 17 image sets out of the whole data set, each representing a routinely obtained full image set (20× and 40× magnification, BF, and all described fluorescence modes) of one aqueous sample. Altogether, 4485 scanning field locations at 40× magnification (3381 at 20× magnification) images are considered in these 17 sets. At 4350 (3132) of these locations, images are acquired. From all scanning points 6.7% ± 9.2 [SD] (8.0% ± 10.4 [SD]) are rejected for darkness. They resulted from bubbles, which are caused by inadequate specimen preparation or by evaporation during sample storage in the plankton chamber, or from residues of the grease paste used for sealing the chambers. Some of this paste sometimes stays stuck to the lid of the plankton chamber and tends to become opaque with time.

Of the acquired images, an average of 3.3% ± 4.2 [SD] (8.0% ± 10.3 [SD]) could not be processed due to an insufficient focusing range. At the beginning of the acquisition (40×), there was a rapid *z*-shift of the plankton chamber bottom, probably caused by temperature changes. This shift was in some specimens too large to be corrected by the refocusing strategy. As the scanning spiral started at edge of the plankton chamber, the preponderance of the defocussed images arose from border scanning points.

Defocussed images at 20× magnification were mainly (6.2%) caused by temperature changes too. The thin bottom of the plankton chamber is not deformed in a regular way, but is strongest in the middle and only weak at the edges. We chose the position for the refocussing at about half of the radius of the chamber, as this procedure should correct these differences adequately. However, toward end of scanning, when shift was maximum, the autofocus range was not always great enough to reach focus. As 20× images were acquired after 40×, this problem occurs predominantly with 20× acquisition in the center of the chamber and rarely at the edge. Increasing the focus range, e.g., to 40 μm diminishes both errors, but increases processing time.

Other minor sources of focus failures were the refraction effects due to bubbles. The refocussing procedure also failed due to darkness by opaque paste or by expanding bubbles. Careful cleaning of the underside of the chamber bottom reduced focus failures. Large lumps of detritus can also mislead the autofocus. However, none of these focus failure sources could be shown in more than one specimen or contributed to more than 0.6% of the defocussed images.

The evaluated specimen represented a wide range of samples characteristics. The procedure was robust regarding character and density of the predominant objects (e.g., round or filamentous algae, detritus).

Nonindividual or Gross Data Evaluation

Probe specific entities such as total numerical density, biomass, or projected area can be derived from all the recorded objects, regardless of whether further discrimination into species or groups of species is done. These quantities are calculated summing up individual entities per measuring area multiplied by the sedimentation chamber area and divided by the water volume used for sedimentation. These measurements are comparable with other global measurements, e.g., absorption acquisition and chlorophyll estimations (Le Floc'h et al., 2002). As they are based on features integrated into the PLASA software, they allow a quick and easy summarizing overview of the samples without performing the elaborate classification of the organisms. In principal, all the measured features could be used like

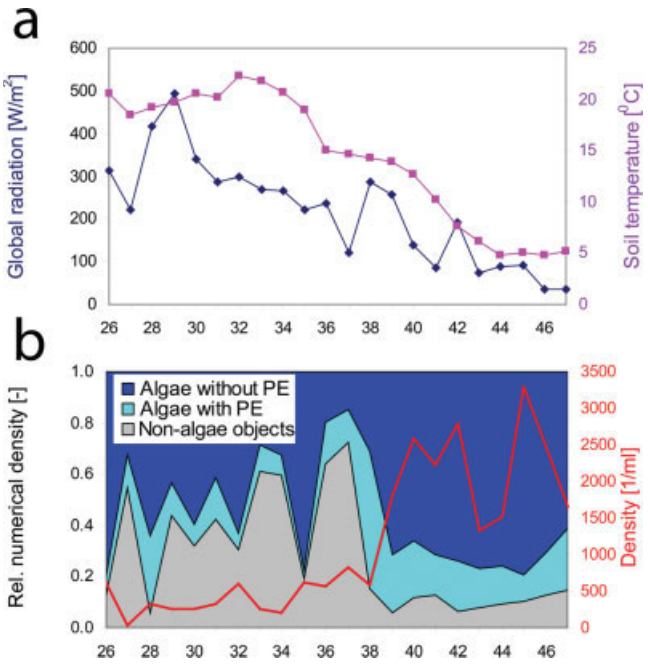

Fig. 7. (**a**) Radiation and temperature near pond 1 during the sampling period. (**b**) Relative numerical density and numerical density of fluorescing objects in Pond 1. Blue: Objects showing fluorescence in channel R_{I3} (chlorophyll a), but not in channel R_{N3} (PE); cyan: Objects with fluorescence in channels R_{I3} and R_{N3}; gray: Objects with fluorescence in channel R_{N3}, but not in channel R_{I3}.

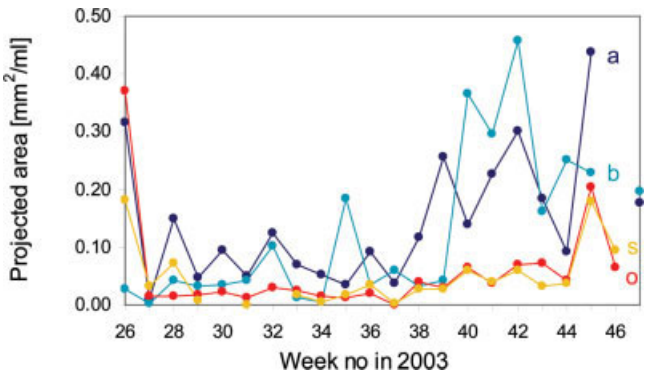

Fig. 8. Projected area of sedimented algae objects per milliliter. Algae were defined by presence of chlorophyll a-fluorescence. Samples were taken from Pond 1 (locations a, b) and Pond 2 (locations c, d).

this (see Appendix), depending on which question is investigated.

In Figures 7 and 8, brief examples are presented for gross data evaluation reflecting the sampling period as well as for a species based analysis. Radiation and soil temperature (as an indicator for water temperature) near pond 1 are outlined in Figure 7a. The nutrient concentrations in the ponds were not measured. The numerical density of all fluorescing objects in Pond 1 showed an increase (Fig. 7b), especially during the last eight sampling weeks. Objects with fluorescence in channel R_{N3} but not in channel R_{I3}, i.e., having fluorescence in the PE channel, but no chlorophyll a fluorescence, in the samples mainly consisted of cell fragments (e.g., of higher plant cell walls). This "PE fluorescence" represents an unspecific fluorescence of mainly organic material, which is also present in many nonplant organisms and which can be used to estimate the amount of detritus. Detritus complicates the algae processing by image analysis, as it can interfere with segmentation by overlapping and, in case of high detritus proportions, a number of false positive classifications of algae species by morphological features can increase.

The relative numerical detritus density varied strongly in Pond 1 during the most of the sampling period, only in the last 8 weeks it remained around 10%. Thus, detritus presented a problem especially during the first half of sampling period. A high detritus proportion, up to 70%, increases the probability of errors and requires that the image analysis is highly discriminative. Subsequently, the numerical density as well as the relative numerical density of algae with and without PE increased and thus the problem with interfering detritus declined. The percentage of algae without PE was small and fluctuated less.

The time course of projected area for the different sampling locations is given in Figure 8. It was higher in Pond 1 during sampling period than in Pond 2. This may reflect the different environments. Generally, the projected area was more similar at both locations in Pond 2 than in Pond 1, possibly indicating a greater exchange between sites.

The biovolume of the exemplarily chosen species is outlined over the sampling period in Figure 9a. Volume was calculated per classified algae according to Hillebrand et al. (1999) using the automatically extracted shape parameters (Appendix Table A1). The example shows that the spherical, large species, as *P. umbonatum* dominates the total biovolume. Some species show seasonal changes (*Trachelomonas* sp.), whereas this was not prominent for *C. marsonii*. Algae with PE (*C. marsonii*, *C. erosa*) seem to be more relevant for biomass than for numerical density.

In Figure 9b, the relation of volume and projected area per milliliter of water of the same data set is shown illustrating its correlation. In contrast to cell density (cells/mL) or relative numerical density, projected area takes the differences in cell size into account, but without strongly focusing on very large species, as the biovolume density (biovolume/mL) does. Projected area correlates well with the biovolume. This holds true for different cells, regardless the exact shape. Only for very extreme shapes as the long, thin filament-like *Ankistrodesmus* sp., ratio of volume and projected area deviates. Thus, projected area enables species-specific as well as a more global analysis. As projected area can be calculated more easily from images than the biovolume, it presents a suitable tool for phytoplankton investigation.

Individual Data Evaluation: Classification of Organisms

The evaluation of the individual classification of all the organisms found is beyond the scope of this article. The automatic detection for a subgroup of organisms

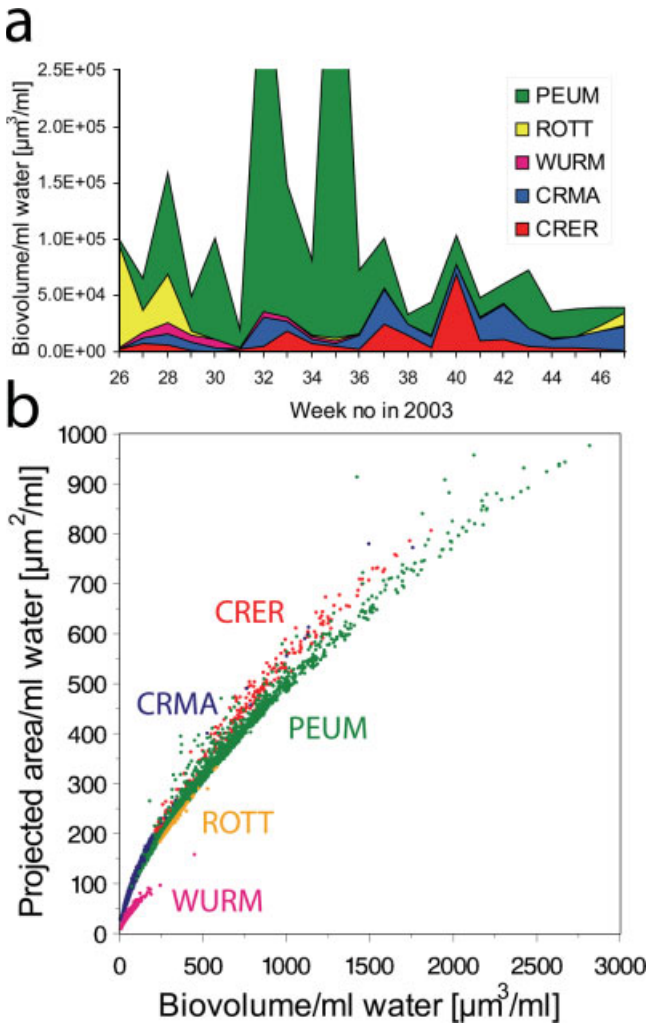

Fig. 9. (**a**) Biovolume of chosen algae species per milliliter. Samples were taken from Pond 1 (locations a, b). (**b**) Scatterplot of the projected area and the biovolume of the data set in Figure 9a.

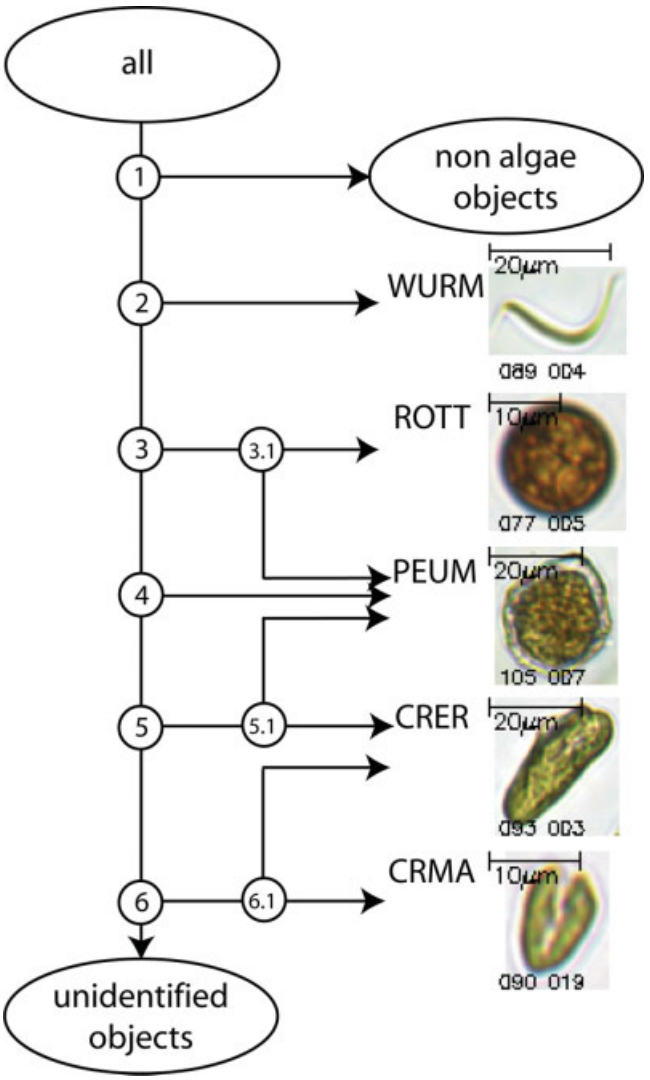

Fig. 10. Tree classifier with decision rules for *Ankistrodesmus* sp. (WURM), *Trachelomonas* sp. (ROTT), *P. umbonatum* (PEUM), *C. erosa* (CRER), and *C. marsonii* (CRMA).

over the span of the sampling period in 2003 is outlined.

The structure of the algae community differs from spring to autumn. Because of this phenomenon, the hierarchical decision tree was built up first with those algae that appeared at the beginning of the year. To ease the change of the classification formula, the classification tree is created by proportionally more univariate than multivariate discrimination steps. In the first samples, the frequency of three groups of algae *Trachelomonas* sp., *Ankistrodesmus* sp., and PEUM was also very high. Diatoms, e.g., occurred later in the year. Also, all nonalgae objects were rejected by lack of fluorescence from chlorophyll a (Fig. 10 step 1).

The *Ankistrodesmus* sp. are sickle or s-shaped algae that appear mostly gray to black. For classification purposes, shape features play the most prominent role. Fluorescence of chlorophyll a must also be present. False-positive objects were generally incorrectly segmented algae, e.g., parts of the border of *P. umbonatum* (see Table 1).

TABLE 1. Classification matrix: results of classification by PLASA (rows) were compared with "true," manual identification (column)

	PEUM	CRER	CRMA	ROTT	WURM	Wrong	Border	Not found
PEUM	1870	17	4	14	0	149	62	252
CRER	4	151	0	0	0	21	8	8
CRMA	1	0	1522	0	0	286	0	47
ROTT	16	0	0	618	0	43	3	24
WURM	0	0	0	0	853	594	0	81

Wrong, false-positive results; Border, algae not correctly classified due to their position on the image border; Not found, false-negative results.

Trachelomonas sp. in our data set is a very homogeneous group. They are circular, middle to dark brown-red with some pattern inside. The fluorescence values are low. False-positive objects were also incorrectly segmented or were small red-brown *P. umbonatum*, which

are classified in step 3.1 (Fig. 10) or were really round artifacts.

The mostly brown colored PEUM have notches on opposite sides, which can be detected only in larger cells. Because of an interior white stripe caused by cell shrinkage during fixation, some segmentation procedures give incorrect results. False-positive objects were produced by *C. erosa* or brown artifacts. *P. umbonatum* are often bright and have no closed border and were therefore not counted. The classification matrix from 23 specimens is outlined in Table 1.

Two types of *Cryptomonas* occur in our data sets. The larger *C. erosa* are predominantly ellipsoid, whereas the smaller *C. marsonii* have different shapes: ellipsoid, drop-shaped, or ellipsoid with one side flattened. The color ranges from yellow-green to dark green. The two algae types were subsequently stepwise separated by area and shape (steps 4 and 5). False-positive objects are frequently green algae or are incorrectly segmented ones. Not detected *Cryptomonas* spp. are often small bright yellow-green or folded. The classification tree for these groups of algae is briefly sketched in Figure 10.

Differentiation of Organisms by Quantitative Parameter Calculation

Fluorescence features as well as morphological features are necessary to discriminate between given algae classes. In addition to biological variations, preparation and sampling variations cause broad feature distributions for different algae classes. The classification results for the five algae are sufficient for *P. umbonatum*, *C. erosa*, *C. marsonii*, and *Trachelomonas* sp. In contrast, *Ankistrodesmus* sp. results in only 58% correct discriminations and therefore needs improvement. However, because of segmentation errors of other algae, high misclassifications could be expected. For the different measurements, the correct classification depends also on the frequency of the algae. The accuracy of the identification of algae species is dependent on the algae properties. For example, thin, only weakly fluorescing algae with varying shapes are difficult to describe by image analysis. *Ankistrodesmus* sp. shows poorer results than the large, uniform algae with high fluorescence (as *P. umbonatum*). Generally, the identification quality as presented in Table 1 was good when compared with the range described for manual counting (e.g., 67–83% self consistency for trained personnel and 43% consensus between trained personnel, 84–95% accuracy for routinely engaged experts) (Culverhouse et al., 2003).

The samples studied were taken from small ponds with comparatively high amounts of detritus, complicating identification as they often fall by accident into morphological defined algae classes and thereby degrade further low counting results. Application of fluorescence information substantially improved separation of algae from nonalgae objects.

DISCUSSION AND CONCLUSIONS

A complete PLASA system is presented for the estimation of population counts of phytoplankton.

Stability of the Acquisition Microscope

Image acquisition was stable during each counting experiment. The principle sources for nonevaluable scanning points were from occluded positions and poorly focused images. Both sources can partially be excluded by adequate and careful sample preparation. Adaptation of the specimen chamber to the surrounding temperature before the start of the acquisition process, e.g., after storage in cool box, reduces the z-shift problem. However, as the nonevaluable data is predominantly caused by technical reasons and not by the sample material, the loss of a low number of scanning points only negligibly affects the statistical analysis of plankton structure.

Position of the Organisms

Organisms often have more than one representation after fixation, e.g., many Bacillariophyceae species assume a girdle or a valve appearance. In these cases, clearly the classifier has to be designed specifically for these structures. However, for the organisms shown and mentioned in this paper, there was no need for multiple representations.

Automatic Segmentation of Organisms

A quantitative estimation of segmentation quality is possible. The conditions for acceptable or erroneous segmentation can be listed and discussed. The segmentation procedure tries to balance on the border between over-exactness and poor identification of organisms. The first can be misguided by shapes when the object is transparent, or is defocussed. The latter causes unmended or disconnected surfaces, for example in the case of slimy organisms or organisms with a thin hull and transparent content. This is especially true for organisms with low contrast in their border zone. It should be remembered that images are gathered in transmitted light instead of phase contrast or dark field imaging, which is highly recommended for transparent objects. The latter would prohibit the use of color parameters that are crucial for several algae types. Also, organisms consisting of several optically weakly connected components are detected as separated, e.g., some *Navicula* spp. and *Cyclotella* spp. or some colony forming algae as several *Ankistrodesmus* spp. Another drawback occurs for touching and occluded objects. In the automatic procedure, no dissection of such objects is performed. This would lead to more erroneous detected objects by over-segmentation. A well-prepared specimen in an adequate amount of water is necessary, where the probe is sampled without disturbance of the sediment to avoid interference by detritus.

Recognizability of Organisms in the Digitized Image

Compared to the direct microscopic view, digitized images are more restrictive. The technical limits of recognition depend on a microscope's properties (resolution, light sensitivity, background noise, etc.) and may even allow an improvement in recognition by light enhancement. Working manually at the

microscope permits the observer to slightly shift focus with the ability to achieve a 3D impression of the object. In contrast, information in digitized images is normally limited to a certain depth-of-field which complicates the identification of the object by a human user as well as by image analysis. Variation of the shown cell plane makes identification especially of large cells often more difficult. Furthermore, the appearance (e.g., colors, contrasts, optical density) of cells is often slightly different to that in the microscope and varies depending on the settings of the image acquisition and image processing. Thus, a human observer used to microscopic work may need some time to become familiar with digitized images. For an unambiguous first identification of most algae species in a study, it is advisable to use the direct microscopic view of living cells as fixation changes the structure of some species (Wetzel and Likens, 1990). However, the chosen preservation mode was tested to minimize deformations in previous tests. Once species are identified, recognition of most algae cells in images is possible.

Adaptability for New Organisms

The classifier can be changed at each node to add a classification step of a new class. If a new algae class or too many misclassified objects appear at a terminal node, feature limits can be reset, or a multivariate discrimination step can be added.

Loss of Organisms

The proposed automated method looses a certain proportion of the cells. Influence of preservation and sedimentation in Utermöhl chamber are discussed elsewhere (Wetzel and Likens, 1990). Generally, there are some losses due to inappropriate fixation and failure of sedimentation e.g., in algae containing gaseous vesicles. Agglutinating of algae and other objects occurs due to filamentous structures or mucilage, making optical as well as image analysis evaluation difficult or even impossible. Major problems in estimating cell number by image analysis occur with occluded, touching, or out-of-focus objects. Filamentous or colony-forming cells as well as very large algae may rise above the focus plane. Some algae form mucilaginous envelopes (e.g., *Cosmarium*) or long mucilaguous stalks or spine like protuberances (e.g., *Cyclotella*, *Micractinium*), thus their cell bodies are located above the focus plane of the other algae. Acquiring z-stacks and aggregating them to a single image with methods as proposed e.g., by Forster et al. (2004) should help solve this problem.

PLASA is a system for complete, automated analysis of phytoplankton structure in field samples, and which includes all steps from sample acquisition to object (algae) recognition and counting. The automated acquisition of representative sets of microscopic images from Utermöhl plankton chambers enables an archiving system of aqueous specimens that have a limited storage time. Every step from acquisition to organism identification and counting has reduced the amount of human interaction time needed if the task were manual. The image analysis system is able to identify a high percentage of the investigated species. Its ability to reject objects has been improved using properties of the autofluorescence.

The use of image analysis for identification and quantification of plankton samples has shown a high potential for speeding up and lowering the costs of environmental investigations, although the diversity of the species and the structure of the samples investigated from aquatic ecosystems make great demands on the image analysis and classifier design. As implementation of new species needs start up time to develop classifiers, PLASA is in the interim suitable for processing of a number of similar samples (e.g., time series of lake or microcosm studies). PLASA combines the advantages of manual counting (high taxonomical resolution) with those of, e.g., flow cytometry (automation, objectivity).

The optical fixation is in contrast to chemical fixation more sustainable, making it suitable for later analysis of new questions or quality assurance. Since PLASA is based on the well-established Utermöhl method, results are comparable with those from manual counting. The use of both BF and fluorescence give complementary as well as additional information and greatly improves separation of algae from each other and from nonalgae objects. Furthermore, the interactive capabilities of PLASA allow the operator to correct or add not correctly detected organisms into the system, provided their acquisition occurs in sufficient number. Also, for visual inspection, a simulation of phase contrast imaging based on the BF image is implemented for observation of the very small organelles.

The system consisting of microscope acquisition and independent image analysis is ready for experiments by external groups. The software analysis system could even be tried with digital data from other acquisition systems provided data and structures necessary for evaluation are adequately adapted.

APPENDIX: FEATURE EXTRACTION

The extracted features are shortly described, listed by their mnemotechnical name and illustrated by an example of *Staurastrum* sp.

TABLE A1. Morphological features

Mnemonic	Number	Description
General shape		
A, A1	35, 14	Area in pixels by count, area by integration over the contour points
P, P2A	36, 37	Perimeter, shapefactor $p2a = \frac{P^2}{4\pi A}$
Xmin, Xmax, Ymin, Ymax	27–30	Box coordinates of the object
BA, BANZ, bamax, basd, bdthr	61, 68–70, 60	Bright partition by threshold bdthr: area, number of connected components, area of maximum component, SD of areas of comp.
DA, DANZ, damax, dasd, bdthr	62, 75–77, 60	Dark partition by threshold bdthr: area, number of connected components, area of maximum component, SD of areas of comp.
CA	78	Area of center area by erosion
bia	141	Area of inner rim ($A = bia + CA$)
Significant points		
Kx, Ky	11, 12	Centroid coordinates
msc_rad, msc_x, msc_y	118, 142, 143	Minimum spanning circle (Datta, 1999): radius, location of center
mx_EXT, kx1, ky1, kx2, ky2	38–42	Maximum extension, location of extremum points
rad rad_kx, rad_ky	43–45	Maximum inscribable circle; radius, location of center
poa pox, poy pota, pono	52–56	Regions disappeared by opening: area of maximum region, centroid of maximum region, total area, number of regions
Principal components		
pc_ew1, pc_ew2, pc_ev1x, pc_ev1y, pc_ev2x, pc_ev2y, pc_thet	151–157	Principal components analysis: first two eigenvalues, locations and angle of the eigenvectors
Convex hull		
a_ch, def	116, 117	Area, deficiency of convex hull region
Contour spectrum		
sp1rm6 sp1im6, . . ., sp1rm1, sp1im1, sp1r0, sp1i0, sp1rp1, sp1ip1, . . ., sp1rp6, sp1ip6	90–115	Complex spectrum [−6, 0, 6] from Fourier ($\mathcal{F}$) transformed complex (periodic) contour function $c(p) = x(p) + iy(p)$ $\mathrm{sp}(p) = \mathcal{F}(c(p))$; $p \in [0, P]$(P perimeter) with $\mathrm{sp}(X) = \mathrm{sp1}rX + i \cdot \mathrm{sp1}iX$; $X \in [-(m)6, (p)6]$
Fourier descriptor features		
el1_a, el1_mn, el1_mx, el1_dea, el1_fac, el1_shx, el1_shy	144–50, 87–89	Ellipse from complex spectrum sp([−1, 0, 1]) of contour: area, length minimum, maximum axis, deviation area, size factor, location of center
el1_stw, el1_ff, el1_efd	87–89	Spatial step width, Fourier feature, energy (da Fontoura Costa and Cesar 2001, p.465)

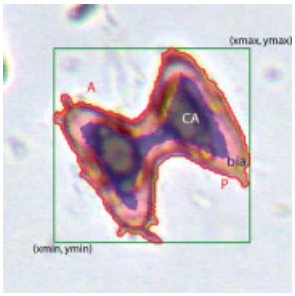

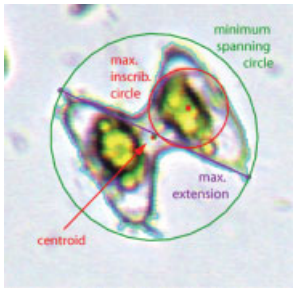

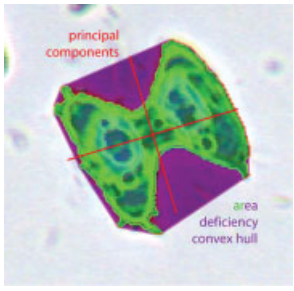

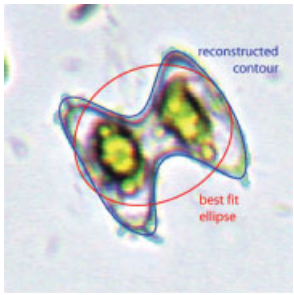

TABLE A1. (continued)

Mnemonic	Number	Description
Invariant shape moments		
lmM1-lmM7	20–26	Moments from object points (Hu, 1962)
lm1-lm7	3–9	Moments from object points weighted by density (Hu, 1962; Rodenacker and Bengtsson, 2003)
nm1-nm4, mm1-mm4, cnm1-cnm3	119–129	Invariant moments from object points (Reiss, 1993)
nim1-nim4, mim1-mim4, cnim1-cnim3	130–140	Invariant moments from object points weighted by density (Rodenacker and Bengtsson, 2003; Reiss, 1993)
Freeman contour code features		
fmbe	57	Curvature calculation from freeman chain code Bending energy: sum of squared curvatures
fmtac	58	Total absolute curvature
fmnp	59	Number of Freeman contour points

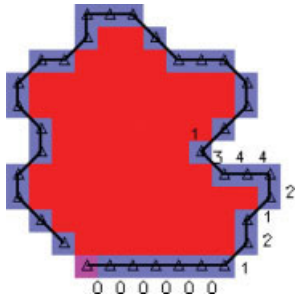

TABLE A2. Densitometric features

Mnemonic	Number	Description
Extinction		$E = -\log_{10}\left[\frac{I_{SC}}{\text{mode}(I_{SC})}\right]^{a}$
M00, M1-M4	10, 31–34	Total extinction, mean, standard deviation, skewness, excess of *object* extinction values
bia, BIM1-M4	141, 83–86	area, mean, standard deviation, skewness, excess of *border* extinction values
CA, CM1-M4	78–82	*center* extinction values
BA, BM1-M4	61, 64–67	*bright* extinction values
DA, DM1-M4	62, 71–74	*dark* extinction values
boa, BOM1-M4	158–162	*near background* extinction values

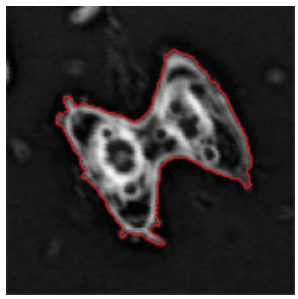

[a]I_{SC}: Intensity, shading and color corrected.

TABLE A3. Colorimetric features

Mnemonic	Number	Description
Colorimetry		
LUMM1-M4	201–204	Mean, standard deviation, skewness, excess of luminance values (HLS transformation)
SATM1-M4	163–166	saturation values (HLS transformation)
HUEM1-MD1	167–170	hue values M_1, SD_1, M_2, SD_2, $mode_1$ (HLS transformation)
LABM1-M4	187–190	luminance values (Lab transformation)
CHROM1-M4	191–194	saturation values (Lch transformation)
HUE1M1-MD1	195–198	hue values M_1, SD_1, M_2, SD_2, $mode_1$ (Lch transformation)

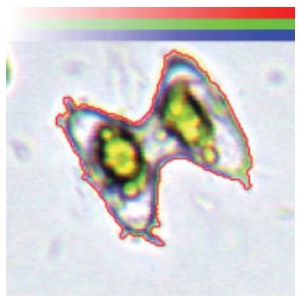

TABLE A4. Fluorescence features

Mnemonic	Number	Description
Fluorimetry		$F = -\log_{10}\left[1 - \frac{FI - FI_{BC}}{n_i 255}\right]^{a}$
FLU1M1-M4	171–174	Mean, standard deviation, skewness, excess of red 13 fluorescence values
FLU2M1-M4	175–178	green 13 fluorescence values (see Image acquisition method)
FLU3M1-M4	179–182	red N3 fluorescence values
FLU4M1-M4	183–186	red M3 fluorescence values

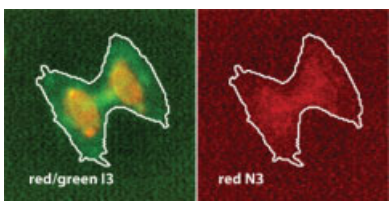

[a]*FI*, Integrated fluorescence intensity; n_i, integration number of frames.

TABLE A5. Feature transformations

Formula	Description
$TOT\ldots = \ldots M1\ldots .A$	Total . . . (intensity, density, fluorescence)
$P2A = \frac{P^2}{4\pi A}$	Shapefactor
$\frac{msc\_rad}{rad}$	Measures of extension and relativity
$el1r = \frac{el1\_mn}{el1\_mx}$	Circularity Ellipticity
$chaa = \frac{a}{a\_ch}$	Convexity
$defach = \frac{def}{a\_ch}$	Convexity
$deaa = \frac{el1\_dea}{A}$	Ellipticity
$baa = ba/A$	Relative bright compartment
$daa = da/A$	Relative dark compartment
$\frac{[(Kx,Ky)-(msc\_x,msc\_y)]}{msc\_rad}$	Deviation of centroid from minimum spanning circle
$\frac{[(Kx,Ky)-(rad\_kx,rad\_ky)]}{msc\_rad}$	from maximum inscribable circle
$\frac{[(Kx,Ky)-(el1\_shx,el1\_shy)]}{msc\_rad}$	from ellipse center

ACKNOWLEDGMENTS

For the development of the IDL programs, the first author thanks the IDL community, especially David Fanning (http://www.dfanning.com) and many news list contributors (news:comp.lang.idl-pvwave). The authors thank the Institute of Soil Ecology, GSF, for access to their pond (Pond 1). The method of image acquisition (optical fixation) is partly covered by the German patent application DE 100 53 202 A 1.

REFERENCES

Babichenko S, Kaitala S, Leeben A, Poryvkina L, Seppälä J. 1999. Phytoplankton pigments and dissolved organic matter distribution in the gulf of riga. J Mar Syst 23:69–82.

Bayerand MM, Droop SJM, Mann DG. 2001. Digital microscopy in phycological research, with special reference to microalgae. Phycol Res 49:263–274.

Culverhouse PF, Williams R, Reguera B, Herry V, Gonzalez-Gil S. 2003. Do experts make mistakes? A comparison of human and machine identification of dinoflagellates. Mar Ecol Prog Ser 247:17–25.

da Fontoura Costa L, Cesar RM, Jr. 2001. Shape analysis and classification: Theory and practice. Image processing series. Boca Raton: CRC Press.

Datta A. 1999. On some self-organizing models and their applications, Dissertation, Indian Statistical Institute, Calcutta.

Formaggio E, Cinque G, Bassi R. 2001. Functional architecture of the major light harvesting complex of photosystem. J Mol Biol 314: 1157–1166.

Forster B, Van De Ville D, Berent J, Sage D, Unser M. 2004. Extended depth-of-focus for multi-channel microscopy images: A complex wavelet approach. In: Proceedings of the second 2004 IEEE International Symposium on Biomedical Imaging: From nano to macro (ISBI'04), April 15–18, Arlington, VA, USA.

Franqueira D, Orosa M, Torres E, Herrero C, Cid A. 2000. Potential use of flow cytometry in toxicity studies with microalgae. Sci Total Environ 247:119–126.

Gaston KJ, O'Neill MA. 2004. Automated species identification: Why not? Philos Trans R Soc Lond B Biol Sci 359:655–667.

Gray AJ, Young D, Martinand NJ, Glasbey CA. 2002. Cell identification and sizing using digital image analysis for estimation of cell biomass in high rate algal ponds. J Appl Phycol 14:193–204.

Hense BA, Welzl G, Severin GF, Pfister G, Behechti A, Schramm K-W. 2003. Effects of 4-nonylphenol on phytoplankton and periphyton in aquatic microcosms. Environ Toxicol Chem 22: 2727–2732.

Hense BA, Severin GF, Welzl G, Schramm K-W. 2004. Effects of 17a-ethinylestradiol on zoo- and phytoplankton in lentic microcosms. Anal Bioanal Chem 378:716–724.

Hillebrand H, Dürselen CD, Kirshtel D, Pollingher U, Zohary T. 1999. Biovolume calculation for pelagic and benthic microalgae. J Psychol 35:403–424.

Hu MK. 1962. Visual pattern recognition by moment invariants. IRE Trans IT 8:179–187.

International Telecommunication Union-R. 1990. Basic parameter values for the standard for the studio and for international programme exchange. Technical Report, ITU-R Recommendation BT.709, ITU, Geneva. (Formerly CCIR Rec. 709).

Kittler J, Illingworth J, Foglein J. 1985. Threshold selection based on a simple image statistic. Comp Vision Graph Image Proc 30:125–147.

Larkum AWD, Douglas SE, Raven JA. 2003. Advances in photosynthesis and respiration, Vol 14: Photosynthesis in algae. London: Kluwer.

Le Floc'h E, Malara G, Sciandra A. 2002. An automatic device for in vivo absorption spectra acquisition and chlorophyll estimation in phytoplankton cultures. J Appl Phycol 14:435–444.

Lund JWG, Kipling C, Le Cren ED. 1958. The inverted microscope method of estimating algal numbers and the statistical basis of estimations by counting. Hydrobiologia 11:143–170.

Reiss TH. 1993. Recognizing planar objects using invariant image features. Berlin: Springer-Verlag.

Rines J. 1999. Phytoplankton imaging and analysis systems: Instrumentation for field and laboratory acquisition, analysis and www/lan-based sharing of marine phytoplankton data (DURIP). Technical Report, Graduate School of Oceanography, University of Rhode Island, South Ferry Road, Narragansett, Rhode Island 02882-1197. Available at http://www.gso.uri.edu/criticalscales/program/investig/rines/BCRINEB.PDF

Rodenacker K, Bengtsson E. 2003. A feature set for cytometry on digitized microscopic images. Anal Cell Pathol 25:1–36.

Rowan KS. 1989. Photosynthetic pigments of algae. Cambridge: Cambridge University Press.

Serra J. 1982. Image analysis and mathematical morphology. London: Academic Press.

Steinberg CE, Schäfer H, Siedler M, Beisker W. 1996. Ataxonomic assessment of phytoplankton integrity by means of flow cytometry. Arch Toxicol Suppl 18:417–434.

Utermöhl H. 1958. Zur Vervollkommnung der quantitativen Phytoplanktonmethodik. Mitt Int Ver Limnol 9:1–38.

Walker RF. 1999. Cyanobacteria detection and species classification by image analysis; cyanobacterial risk assessment for lake biwa (crab) project. Final report, Japan Science and Technology Agency (Japan), Lake Biwa Research Institute, Otsu, Japan. Available at http://dr_ross_f_walker.tripod.com/STAFinalReport/STAFinalReport.zip

Walker RF, Tsujimura S, Kumagai M. 1998. Automated monitoring of six cyanobacterial taxa from lake biwa by image processing. Technical Report, SIL '98, the 27th Congress of the International Association of Limnology, Dublin, Ireland. Available at http://www.koitsu.com/texture/SILPaper.zip

Walker RF, Ishikawa K, Kumagai M. 2002. Fluorescence-assisted image analysis of freshwater microalgae. J Microbiol Methods 51:149–162.

Wetzel RG, Likens GE. 1990. Limnological methods. New York: Springer-Verlag.